Human Interaction and Emerging Technologies (IHIET-AI 2025), Vol. 161, 2025, 485–495
https://doi.org/10.54941/ahfe1005941

Advances in Pulse Rate Variability (PRV) Monitoring With rPPG: Insights From Unsupervised Methods

Marc Escrig-Villalonga[1], Ursula Martinez-Iranzo[1], Cristina Herrera-Ligero[1], Alberto Albiol[2], and Ana de la Torre-García[1]

[1]Digital Health Department, Instituto de Biomecánica de Valencia, Universitat Politècnica de València, València, 46022, Spain
[2]PRHLT Research Centre, Universidad Politécnica de València, Valencia, 46022, Spain

ABSTRACT

Remote photoplethysmography (rPPG) emerges as a non-invasive alternative for pulse and pulse rate variability (PRV) measurement, eliminating the need for direct skin contact. This approach is particularly suitable for applications where wearable sensors are impractical, such as the automotive sector, where accurate and robust PRV monitoring is essential to enhance driver safety by providing real-time insights. This study evaluates the accuracy and robustness of rPPG signal extraction using the Freyja/IBV-Dataset, which comprises 73 participants with diverse intrinsic factors, such as age, body mass index (BMI), and skin phototypes, as well as extrinsic conditions, including varying lighting and distances. Seven rPPG algorithms (GREEN, POS, CHROM, ICA, FastICA, PVB, and LGI), selected for their established efficacy in handling environmental variations, were compared against electrocardiogram (ECG) as the reference standard. The findings reveal that the mean normal-to-normal interval (meanNNI) demonstrates the greatest robustness when estimated using ICA and FastICA, which achieved consistently low mean absolute errors (MAE) even under challenging conditions such as reduced lighting and increased distance. However, the estimation of the standard deviation of normal-to-normal intervals (SDNN), a parameter sensitive to noise and environmental conditions, showed higher errors. These discrepancies are attributed to intrinsic differences between mechanical (rPPG) and electrical (ECG) signals, disparities in sampling frequencies between devices, and environmental influences. This study highlights the need to optimize rPPG signal extraction and processing techniques to improve the accuracy and robustness of PRV parameter estimation. Future research should focus on increasing the image sampling rate, exploring PPG measurements closer to the face, and employing advanced artificial intelligence (AI) methods to adapt algorithms for challenging conditions, such as diverse skin phototypes and complex environmental settings.

Keywords: Pulse rate variability (PRV), Remote photoplethysmography (RPPG), Unsupervised extraction methods, Automotive safety, Driver monitoring, Health monitoring, Physiological state

INTRODUCTION

Monitoring the physiological state of drivers in real-world automotive environments is important to enhance road safety and improve driving performance. Among various physiological markers, pulse rate variability (PRV) has emerged as a critical indicator for assessing stress, fatigue, and cognitive load behind the wheel (Burlacu et al., 2021). Traditional photoplethysmography (PPG) methods, although reliable, rely on contact-based sensors that can be impractical in real-world automotive environments.

Remote photoplethysmography (rPPG) provides a promising alternative by leveraging standard video cameras to extract pulse-related signals from subtle colour variations in the driver's skin. Unlike contact-based sensors, rPPG enables fully non-invasive PRV measurement, offering a more natural and seamless integration into automotive systems. However, the viability of using unsupervised rPPG algorithms for PRV estimation under dynamic conditions—such as variable lighting, driver movement, and skin tone diversity—remains largely unexplored.

Current approaches to rPPG generally fall into two main categories: unsupervised (non-learning-based) methodologies that apply well-established signal processing and computer vision techniques, and deep learning-based methods that rely on large annotated datasets. While these strategies have shown promise in controlled environments, their performance often degrades under the dynamic conditions encountered in actual driving scenarios (Wang et al., 2024).

To our knowledge, this study is the first to systematically compare PRV parameters across multiple unsupervised rPPG algorithms, including GREEN, POS, CHROM, ICA, FastICA, PVB, and LGI. These methods were selected based on their prevalence in the literature and their capacity to handle environmental and demographic variations. Using the newly developed Freyja/IBV-Dataset, which encompasses diverse age groups, BMI ranges, and skin phototypes, we assess the performance of these algorithms in estimating PRV parameters under realistic conditions.

This investigation aims to evaluate the feasibility of unsupervised rPPG algorithms for accurate PRV estimation, providing critical insights into their robustness and reliability in real-world scenarios. By highlighting the strengths and limitations of these methods, this study contributes to the foundation for developing more effective and practical driver monitoring systems.

MATERIALS AND METHODS

Data Collection

A new dataset (Freyja/IBV-Dataset) of 73 subjects (35 females and 38 males) with ages ranging from 18 to 85, covering the 6 skin phototypes according to the Fitzpatrick scale (Sachdeva, 2009), and BMI ranging from 15 to 40, was acquired.

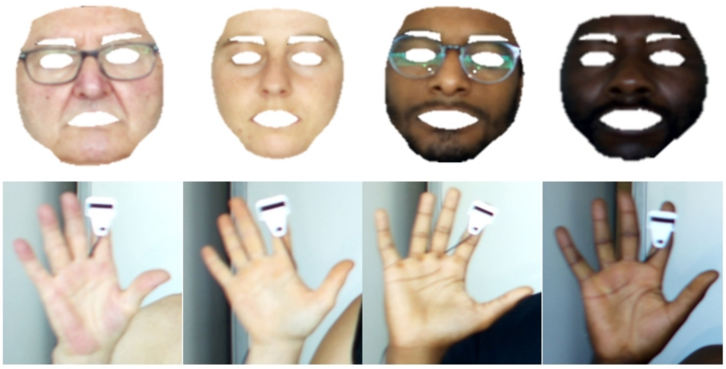

Figure 1: Sample of the Freyja/IBV-Dataset, illustrating diversity in skin phototypes (top row) and hand features (bottom row).

In order to determine the sample size, specific ranges have been defined for each of the intrinsic subject factors (Table 1) and all possible combinations have been covered. The sample is balanced in terms of age and sex, while the distributions for BMI and phototypes follow a normal (Gaussian) distribution.

Table 1. Participant distribution by gender, age, BMI, and Fitzpatrick phototype, with percentages relative to the total sample.

Factor	Subgroup	N	(%)
Gender	Female	35	47.9
	Male	38	52.1
Age	18–50	39	53.4
	51–85	34	46.6
BMI	<21	11	15.1
	21–29	42	57.5
	>29	20	27.4
Fitzpatrick phototype	I-II	20	27.4
	III- IV	37	50.7
	V-VI	16	21.9

Four measurements were taken modifying the distance between the subject and the equipment (1 m and 2 m) and the entrance of natural light (presence or absence of natural light). The subject remained seated and instrumented throughout the sessions. The forehead, face and lower neck were exposed to the cameras. Prior to each measurement, the ambient light condition was recorded using a luxmeter. Subjects were required to remain still and quiet, breathing normally. They also had to raise their hands to the level of their heads with the right palm facing forward, as shown in Figure 1. At the beginning and at the end of each recording, systolic and diastolic blood pressure were measured with the Withings BPM Connect WPM05 digital sphygmomanometer. SpO2 was measured with WristOx2 Model 3150 wrist-worn pulse oximeter.

During each recording session, two cameras, one RGB and one NIR, were used to capture images synchronously with a resolution of 1920x1080 pixels at a sampling rate of 60 Hz and 15 Hz, respectively. Image capture was synchronised with the acquisition of electrocardiogram (ECG) and respiration signals. For this purpose, the BiosignalsPlux (*PLUX Biosignals*, n. d.) acquisition system was used together with a respiratory band and ECG sensors disposed in the Lead I. Throughout the recording, a 640 nm laser with a dot pattern (classified as eye-safe, RPPES, class 1M) was activated. To capture this pattern, the NIR camera was equipped with an optical filter of the same wavelength.

The procedure described in this work is part of the initiative registered on ClinicalTrials.gov under the ID NCT05947721. The experimental protocol was approved by the ethics committee of the Universitat Politècnica de València (UPV) P01_25-05-2022, and all participants signed an informed consent for the execution of the trial and use of their data.

rPPG Signal Extraction

Extracting the RGB signal is the preliminary step before applying algorithms designed to derive the rPPG signal. For each captured image, the FaceMesh segmenter (Grishchenko et al., 2020) was employed to accurately identify and segment the facial skin regions. The mean pixel values within these segmented areas were calculated to generate the RGB input required for subsequent analysis by rPPG algorithms. Each of the RGB channels was further processed to remove baseline trends using the detrend function from SciPy (Virtanen et al., 2020).

To evaluate the quality and performance of rPPG signal extraction, seven unsupervised methodologies were applied: GREEN (Verkruysse et al., 2008), POS (Wang et al., 2017), ICA (Poh et al., 2011), FastICA (Hyvärinen & Oja, 1997), CHROM (de Haan & Jeanne, 2013), LGI (Pilz et al., 2018), and PVB (Haan & Leest, 2014). These algorithms were selected based on their proven applicability in previous studies and their capacity to handle variations in illumination, motion artifacts or skin tone differences. All implementations were performed using the rPPG-Toolbox (Liu et al., 2023), a standardized open-source framework designed for the comparative analysis of rPPG techniques. The key principles underlying each of these algorithms are summarized in Table 2, which provides a detailed description of their mechanisms and computational approaches.

Table 2. Description of the unsupervised rPPG signal extraction algorithms.

Algorithm	Principle
GREEN	Exploits green channel intensity variations for rPPG signal extraction.
POS	Plane-orthogonal-to-skin (POS) algorithm that finds pulsatile signals in an RGB normalized space orthogonal to the skin tone.

Table 2. Continued

Algorithm	Principle
CHROM	Chrominance-based method (CHROM) to separate the specular reflection component from the diffuse reflection component, which contains pulsatile physiological signals, both reflected from the skin and based on the dichromatic reflection model.
ICA	Independent Component Analysis (ICA) to uncover the independent source signals.
FastICA	An optimized version of ICA that employs iterative fixed-point algorithms to extract independent components efficiently, reducing computational complexity while maintaining signal integrity.
PVB	Pixel Variance Balancing (PVB) algorithm emphasizes balancing the variance of pixel intensities across consecutive frames, mitigating motion artifacts and ensuring more stable rPPG signal extraction.
LGI	Local Group Invariance (LGI) method, a stochastic representation of the pulse signal based on a model that leverages the local invariance of the heart rate as a quasi-periodical process dynamics and obtained by recursive inference to remove extrinsic factors such as head motion and lightness variations.

Signal Refinement and IBIs Extraction

A fourth-order Chebyshev Type II bandpass filter was applied to enhance the quality of the rPPG signal and ensure reliable RR interval extraction. The filter's cut-off frequencies were set at 0.33 Hz (20 beats per minute, bpm) and 4 Hz (240 bpm), covering the physiological range of human heart rates. Filtering was performed after the RGB-to-rPPG transformation, following recommendations in the literature that emphasize the benefits of post-transformation filtering for improving signal clarity and reducing noise (Guler et al., 2023).

The rPPG signal is processed to extract inter-beat intervals (IBIs) by identifying systolic peaks corresponding to each pulse. This process employs a specialized function that detects relative maxima in the signal, which are determined by comparing each point with its neighbours within defined segments. An adjustable quality criterion, based on the maximum tolerable error relative to the original signal, is applied to validate the detected maxima. This ensures that the identified peaks faithfully represent the underlying rPPG signal. To further enhance robustness, the function operates within a sliding window of 10 seconds, reducing the impact of high-amplitude outliers that could mask true systolic peaks.

To ensure the physiological plausibility of the extracted IBIs, outliers corresponding to heart rates outside the physiological range (30–200 beats per minute) were first removed, eliminating implausible intervals prior to further analysis. Subsequently, an iterative filtering approach was applied to refine the detected peaks and validate the remaining intervals. This process dynamically adjusted the acceptable range for IBIs based on the mean and standard deviation of the most recent valid intervals, enabling the identification and correction of aberrant intervals. Intervals exceeding the upper or lower bounds were excluded from the analysis, and the process continued iteratively until all remaining intervals fell within the predefined range. Linear interpolation was then used to reconstruct a continuous IBI sequence.

The ground truth IBI sequences were derived from the synchronously recorded ECG signals, which were pre-processed using the Pan-Tompkins algorithm (Pan & Tompkins, 1985). This method enhances QRS complexes while suppressing noise, baseline wander, and high-frequency artifacts, ensuring accurate identification of R peaks. The same peak detection algorithm applied to the rPPG signal was used for the filtered ECG signal.

The resulting IBIs sequences were further refined through the same iterative dynamic filtering approach was applied to the rPPG-derived IBIs to refine the sequence by excluding implausible intervals and ensuring that all remaining intervals fell within the predefined range, thereby maintaining consistency between the ground truth and the rPPG-derived IBIs.

PRV Parameters, Evaluation Metrics and Results

This study concentrated on time-domain PRV parameters due to their proven reliability in short-term recordings (Shaffer et al., 2020). Frequency-domain and non-linear parameters were excluded because of their susceptibility to noise and their limited applicability to short recording segments. Among the time-domain parameters, we selected the two most informative indices of PRV—Mean of Normal-to-Normal Intervals (meanNNI) and Standard Deviation of Normal-to-Normal Intervals (SDNN)—as they are considered robust metrics. These measures provide a comprehensive understanding of both the central tendency and variability of heart rate dynamics, making them particularly well-suited for the study's emphasis on short-term recordings.

To ensure the quality and reliability of the rPPG signals analysed in this study, specific criteria were established to exclude recordings with insufficient signal quality or excessive artifacts. Recordings were excluded if the number of detected peaks in the rPPG signal differed by more than 20% from the corresponding ground truth ECG signal or if more than 40% of the detected peaks in the signal are removed after iterative filtering of the IBI vector. Table 3 presents the percentage of recordings excluded under these conditions for each algorithm and experimental setup.

Table 3. Percentages of excluded recordings out of the total in the demographic and experimental subgroups. For each subgroup, the best result is highlighted in bold.

Factor	Subgroup	% Excluded Records						
		GREEN	POS	CHROM	ICA	FastICA	PVB	LGI
Gender	Female	**7**	24	37	9	8	28	40
	Male	11	37	52	**9**	11	20	38
Age	18–50	**12**	36	46	**12**	13	28	39
	51–85	**5**	23	43	6	**5**	19	39

Table 3. Continued

Factor	Subgroup	% Excluded Records						
		GREEN	POS	CHROM	ICA	FastICA	PVB	LGI
BMI	<21	**3**	24	43	**3**	5	16	38
	21–29	9	32	44	9	**8**	23	42
	>29	**13**	29	46	**13**	14	30	33
Fitzpatrick phototype	I-II	**6**	21	35	**6**	9	17	27
	III- IV	**2**	27	48	3	3	24	37
	V-VI	28	47	47	25	**24**	33	56
Lighting	Good	7	20	34	**6**	7	10	37
	Low	**11**	40	55	12	12	39	41
Distance	1 meter	8	29	39	**7**	9	22	37
	2 meters	**10**	31	50	11	**10**	26	41

Mean Absolute Error (MAE) was calculated for each algorithm across varying environmental conditions as well as for each demographic subgroup. These MAE values are summarized in Table 4 for meanNNI values and in Table 5 for SDNN values, providing a comprehensive overview of performance across groups. To further analyse variations in MAE, non-parametric statistical tests were conducted: the Kruskal-Wallis (Kruskal & Wallis, 1952) test was employed for categories with more than two levels due to its robustness for non-normally distributed data, and the Mann-Whitney U test (Mann & Whitney, 1947) was used for pairwise comparisons where normality could not be assumed. Dunn's post hoc (Dunn, 1964) tests were performed when statistically significant differences ($p < 0.05$) were identified, allowing for the determination of specific group differences. Type I statistical error was taken into account to ensure the robustness of the findings using Bonferroni correction for multiple comparisons.

Table 4. MAE of meanNNI across demographic and environmental subgroups, with statistically significant differences ($p < 0.05$) marked with an asterisk. For each subgroup within each factor, the best result is highlighted in bold.

Factor	Subgroup	MAE meanNNI (ms)						
		GREEN	POS	CHROM	ICA	FastICA	PVB	LGI
Gender	Female	24	74	77	**16**	25	59	47
	Male	16	66	51	**10**	14	57	37
Age	18–50	24*	62	55	**16**	20	62	45
	51–85	15*	77	70	**9**	19	52	39
BMI	<21	24	79	48	**9**	15*	57	49
	21–29	18*	73	70	**16***	26*	56	44
	>29	13*	56	52	**8***	**8***	49	33
Fitzpatrick phototype	I-II	16*	67	50	**10***	15	62	45
	III- IV	16*	80*	73	**8***	14*	51	38
	V-VI	38*	43*	56	**30***	42*	69	49
Lighting	Good	17	56	60	**9**	16	50	25
	Low	23	88	65	**16**	23	66	67
Distance	1 meter	21	66	59	**12**	16	58	36
	2 meters	18	73	65	**14**	24	57	48

Table 5. MAE for SDNN across demographic and environmental subgroups, with statistically significant differences ($p < 0.05$) marked with an asterisk. For each subgroup within each factor, the best result is highlighted in bold.

Factor	Subgroup	MAE SDNN (ms)						
		GREEN	POS	CHROM	ICA	FastICA	PVB	LGI
Gender	Female	106	207	224	**79**	94	187	160
	Male	96	196	194	**71**	90	217	153
Age	18–50	114*	195	191*	**87***	99*	213	164
	51–85	87*	207	226*	**61***	83*	188	149
BMI	<21	112*	199	182	**73***	95*	233	169
	21–29	107*	205*	220	**82***	101*	205	161
	>29	81*	195*	194	**62***	68*	181	137
Fitzpatrick phototype	I-II	93*	206	200	**69**	84*	216	160
	III- IV	90*	207*	219	**64***	87*	191	147
	V-VI	145*	176*	192	**113***	116*	209	176
Lighting	Good	92	184	204	**70**	82	187	108
	Low	110	224	212	**80**	101	218	228
Distance	1 meter	99	200	205	**71**	89	203	129
	2 meters	103	202	210	**79**	95	200	186

In the case of meanNNI, GREEN, ICA, and FastICA stood out for their higher consistency, showing lower MAE across nearly all subgroups and maintaining a low percentage of excluded recordings. In particular, ICA demonstrated remarkable robustness against variations in distance and lighting conditions. In contrast, POS, CHROM, PVB, and LGI exhibited significant increases in MAE, as well as a higher number of excluded segments under poor lighting conditions, reflecting greater vulnerability to signal quality degradation.

The evaluated camera distance did not produce significant changes in the performance of most algorithms, except for CHROM, which experienced a notable increase in the percentage of excluded recordings. Regarding demographic variables such as gender and age, the detected statistical differences did not translate into substantial MAE increases compared to other algorithms, with discrepancies more attributable to the percentage of excluded segments.

Statistical analysis revealed significant differences ($p < 0.05$) in the meanNNI parameter between certain demographic subgroups. Specifically, significant differences were observed between subjects with phototypes I-II or III-IV and those with phototypes V-VI. Additionally, the generalized increase in MAE and the higher percentage of excluded recordings in individuals with darker phototypes highlight the need to develop algorithms that adapt to variations in skin pigmentation. Although the CHROM and PVB algorithms did not present significant differences between these subgroups, their MAE and percentage of excluded recordings were higher compared to other algorithms. Furthermore, the analysis of groups based on BMI showed significant differences in the FastICA, ICA, and GREEN algorithms; however, the differences in MAE between the groups were not particularly pronounced.

In the SDNN analysis, ICA, FastICA, and GREEN again demonstrated better performance, with lower MAE values and greater stability against environmental and demographic changes. However, overall errors were higher than those recorded for meanNNI, indicating that the robustness observed in the first parameter does not always extend to heart rate interval variability. The significant differences detected in SDNN, although similar to those of meanNNI, underscore the need to continue refining extraction methods to improve their performance under challenging conditions.

CONCLUSION

This study evaluated the accuracy and robustness of rPPG signal extraction, considering both intrinsic factors related to the subjects, such as gender, age, BMI and skin phototype, and extrinsic factors, such as lighting and device distance, which can influence the results. Although no single algorithm was identified as optimal for all conditions, ICA and FastICA stood out for their robustness, exhibiting the lowest and most consistent mean absolute errors (MAE), especially in the meanNNI parameter, even in unfavorable lighting and distance contexts. These results highlight the potential of these algorithms for applications such as driving monitoring and other areas requiring reliable estimation of average heart intervals.

However, the estimation of SDNN, which measures heart interval variability, proved to be more affected by noise and experimental conditions, showing higher MAE compared to meanNNI. This difference can be attributed to various factors, such as the dissimilar nature of ECG (electrical) and rPPG (mechanical) signals, disparities in sampling frequencies between contact devices and cameras, signal quality, and environmental influences. These combined factors complicate the precise estimation of non-averaged parameters like SDNN, highlighting the need for further optimization of rPPG algorithms to enhance their accuracy under diverse conditions.

Limitations and Future Research Directions

The main limitations identified in this study include the inherent differences between ECG (electrical) and rPPG (mechanical) signals, as well as the low sampling frequency of images, which particularly affect the precision of the SDNN parameter. Future studies should prioritize increasing the image sampling frequency to better capture signal fluctuations and reduce sampling errors. Additionally, comparing rPPG with PPG signals obtained from areas near the face could help minimize divergences between electrical and mechanical signals.

Additionally, the use of more advanced Artificial Intelligence (AI) models could significantly improve signal extraction by increasing robustness against complex environmental factors and optimizing precision in challenging parameters such as SDNN. This represents a key opportunity to develop more adaptive algorithms applicable in challenging biometric and clinical contexts.

ACKNOWLEDGMENT

This activity has been developed in the framework of the MEDUSA project. MEDUSA is a Technological Network of enginnering applied to the development of intelligent solutions for autonomous movility using a human-centered approach (CER-20231011), Red de Excelencia CERVERA founded by the Ministerio de Ciencia, Innovación y Universidades through the Centro para el Desarrollo Tecnológico y la Innovación E.P.E. (CDTI), using the funding of the The Recovery and Resilience Facility (NextGenEU) from the European Union.

REFERENCES

8-Channel biosignalsplux Kit. (s.f.). PLUX Biosignals. https://www.pluxbiosignals.com/products/8-channel-biosignals-kit

Burlacu, A., Brinza, C., Brezulianu, A., & Covic, A. (2021). Accurate and early detection of sleepiness, fatigue and stress levels in drivers through Heart Rate Variability parameters: A systematic review. Reviews in Cardiovascular Medicine, 22(3), 845–852. https://doi.org/10.31083/j.rcm2203090

de Haan, G., & Jeanne, V. (2013). Robust Pulse Rate From Chrominance-Based rPPG. IEEE Transactions on Biomedical Engineering, 60(10), 2878–2886. IEEE Transactions on Biomedical Engineering. https://doi.org/10.1109/TBME.2013.2266196

Dunn, O. J. (1964). Multiple Comparisons Using Rank Sums. Technometrics, 6(3), 241–252. https://doi.org/10.1080/00401706.1964.10490181

Grishchenko, I., Ablavatski, A., Kartynnik, Y., Raveendran, K., & Grundmann, M. (2020). Attention Mesh: High-fidelity Face Mesh Prediction in Real-time. ArXiv. https://www.semanticscholar.org/paper/Attention-Mesh%3A-High-fidelity-Face-Mesh-Prediction-Grishchenko-Ablavatski/7e627c774997addd7423361e93d8891dd1de35ad

Guler, S., Golparvar, A., Ozturk, O., Dogan, H., & Yapici, M. K. (2023). Optimal digital filter selection for remote photoplethysmography (rPPG) signal conditioning. Biomedical Physics & Engineering Express, 9(2), 027001. https://doi.org/10.1088/2057-1976/acaf8a

Haan, G. de, & Leest, A. van. (2014). Improved motion robustness of remote-PPG by using the blood volume pulse signature. Physiological Measurement, 35(9), 1913. https://doi.org/10.1088/0967-3334/35/9/1913

Hyvärinen, A., & Oja, E. (1997). A Fast Fixed-Point Algorithm for Independent Component Analysis. Neural Computation, 9(7), 1483–1492. Neural Computation. https://doi.org/10.1162/neco.1997.9.7.1483

Kruskal, W. H., & Wallis, W. A. (1952). Use of Ranks in One-Criterion Variance Analysis. Journal of the American Statistical Association, 47(260), 583–621. https://doi.org/10.1080/01621459.1952.10483441

Liu, X., Narayanswamy, G., Paruchuri, A., Zhang, X., Tang, J., Zhang, Y., Sengupta, S., Patel, S., Wang, Y., & McDuff, D. (2023). rPPG-Toolbox: Deep Remote PPG Toolbox (arXiv:2210.00716). arXiv. https://doi.org/10.48550/arXiv.2210.00716

Mann, H. B., & Whitney, D. R. (1947). On a Test of Whether one of Two Random Variables is Stochastically Larger than the Other. The Annals of Mathematical Statistics, 18(1), 50–60. https://doi.org/10.1214/aoms/1177730491

Pan, J., & Tompkins, W. J. (1985). A Real-Time QRS Detection Algorithm. IEEE Transactions on Biomedical Engineering, BME-32(3), 230–236. IEEE Transactions on Biomedical Engineering. https://doi.org/10.1109/TBME.1985.325532

Pilz, C. S., Zaunseder, S., Krajewski, J., & Blazek, V. (2018). Local Group Invariance for Heart Rate Estimation from Face Videos in the Wild. 2018 IEEE/CVF Conference on Computer Vision and Pattern Recognition Workshops (CVPRW), 1335–13358. https://doi.org/10.1109/CVPRW.2018.00172

Poh, M.-Z., McDuff, D. J., & Picard, R. W. (2011). Advancements in Noncontact, Multiparameter Physiological Measurements Using a Webcam. IEEE Transactions on Biomedical Engineering, 58(1), 7–11. IEEE Transactions on Biomedical Engineering. https://doi.org/10.1109/TBME.2010.2086456

Sachdeva, S. (2009). Fitzpatrick skin typing: Applications in dermatology. Indian Journal of Dermatology, Venereology and Leprology, 75, 93. https://doi.org/10.4103/0378-6323.45238

Shaffer, F., Meehan, Z. M., & Zerr, C. L. (2020). A Critical Review of Ultra-Short-Term Heart Rate Variability Norms Research. Frontiers in Neuroscience, 14. https://doi.org/10.3389/fnins.2020.594880

Verkruysse, W., Svaasand, L. O., & Nelson, J. S. (2008). Remote plethysmographic imaging using ambient light. Optics express, 16(26), 21434–21445.

Virtanen, P., Gommers, R., Oliphant, T. E., Haberland, M., Reddy, T., Cournapeau, D., Burovski, E., Peterson, P., Weckesser, W., Bright, J., van der Walt, S. J., Brett, M., Wilson, J., Millman, K. J., Mayorov, N., Nelson, A. R. J., Jones, E., Kern, R., Larson, E., … van Mulbregt, P. (2020). SciPy 1.0: Fundamental algorithms for scientific computing in Python. Nature Methods, 17(3), 261–272. https://doi.org/10.1038/s41592-019-0686-2

Wang, J., Shan, C., Liu, L., & Hou, Z. (2024). Camera-based physiological measurement: Recent advances and future prospects. Neurocomputing, 575, 127282. https://doi.org/10.1016/j.neucom.2024.127282

Wang, W., den Brinker, A. C., Stuijk, S., & de Haan, G. (2017). Algorithmic Principles of Remote PPG. IEEE Transactions on Biomedical Engineering, 64(7), 1479–1491. IEEE Transactions on Biomedical Engineering. https://doi.org/10.1109/TBME.2016.2609282